ACS APPLIED POLYMER MATERIALS

pubs.acs.org/acsapm Article

Functionally Graded Gecko Setae and the Biomimics with Robust Adhesion and Durability

Xiaoxiao Dong,[#] Rui Zhang,[#] Yu Tian,[*] Melvin A. Ramos, Travis Shihao Hu, Zhihang Wang, Hong Zhao, Lipeng Zhang, Yiyang Wan, Zhenhai Xia,[*] and Quan Xu[*]

Cite This: *ACS Appl. Polym. Mater.* 2020, 2, 2658−2666 Read Online

ACCESS | Metrics & More | Article Recommendations | Supporting Information

ABSTRACT: Geckos have the extraordinary ability to adhere and move across varied surfaces, while keeping their tiny high-aspect-ratio foot-hairs intact for thousands of attachment−detachment cycles. Inspired by the dry adhesive structure of gecko sole, various gecko-inspired artificial mimics have been developed, but many of them suffer from premature failures and short fatigue life. Herein, we discover that individual gecko seta is a functionally graded material. Its Young's modulus gradually decreases from base to tip, with up to 20 times of difference in magnitude. Finite element analysis indicates that this gradient design is the key to make the natural setal stalks more flexible (critical for producing large frictional adhesion on rough surfaces) and less stressed (critical for achieving high fatigue resistance) during each attachment. Inspired by these findings, we have fabricated poly(dimethylsiloxane) (PDMS)-based artificial gecko foot-hairs with a gradient distribution of magnetic nanoparticles as the reinforcements, achieving similar varying modulus/stiffness. The biomimetic hairs/pillars show enhanced fatigue resistance compared to the uniform counterparts. This work opens a door in designing dry adhesives with both high adhesive strength and long fatigue life.

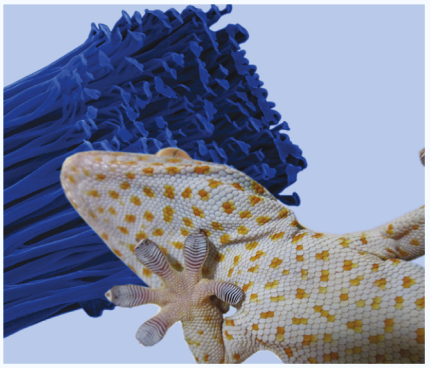

KEYWORDS: *gecko, gradient, durability, magnetic particle, adhesion mechanism*

1. INTRODUCTION

Through millions of years of evolution, living organisms have evolved a variety of intriguing structures with distinctive properties, from which scientists learn to create novel material systems with unprecedented functionalities and performance. Some outstanding examples include, but not limit to, lotus leaves,[1] nepenthes alata,[2] mussel thread,[3] spider silk,[4] ladybird[5] tree frog,[6,7] and gecko feet.[8,9] Among them, geckos have attracted a great deal of attention owing to their strong adhesion,[9] easy detachment,[10] and self-cleaning properties.[11] Relying on these seemingly contradictory properties, geckos can run on smooth or rough, dry or wet surfaces, while retaining their adhesive performance for months between each molting cycle.[12]

It has been shown that van der Waals force alone is sufficient to generate the level of adhesion measured at the animal scale, on the basis of the setal/spatular density, toe pad area, and the force generated by each individual spatulae.[13] Nevertheless, humidity[14] and surface wettability also play a significant role in altering the adhesion via the water bridging effect and/or the influence on the modulus of the keratinous setae.[15−17] Great conformability or flexibility across multiple length scales is of great importance for initiating a firm attachment by many adhesive systems.[18] This is especially true for sticking to surfaces with unpredictable roughness, debris, and contaminants. Geckos and many insects (e.g., beetles and spiders) have adopted the "contact splitting" principle, using high-aspect-ratio and relatively rigid fibrils for achieving reversible and repeatable adhesion. In addition, directionality and anisotropy play a critical role in facilitating easy detachment. Many studies[19−24] have been conducted to mimic the gecko adhesive systems to achieve directional and switchable adhesion similar to that of live geckos. Despite some synthetic dry adhesives achieve 10 times adhesive strength than the gecko hairs,[25] the artificial mimics still substantially lag behind the natural counterpart in terms of durability and reusability. Further understanding of the fundamental principles in gecko adhesive systems, especially pertaining to longevity and fatigue resistance is in high demand.

One of the phenomena, commonly observed across different organisms, is the presence of functionally graded fibrils and structures. It plays a critical role in strengthening the biological structures and achieving multifunctionality.[26] For instance, the cacti Opuntia microdasys can survive in arid environment, using multistructural spines featuring geometrical gradient and

Received: March 19, 2020
Accepted: June 3, 2020
Published: June 3, 2020

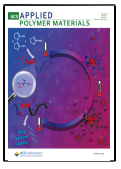

https://dx.doi.org/10.1021/acsapm.0c00282
ACS Appl. Polym. Mater. 2020, 2, 2658−2666

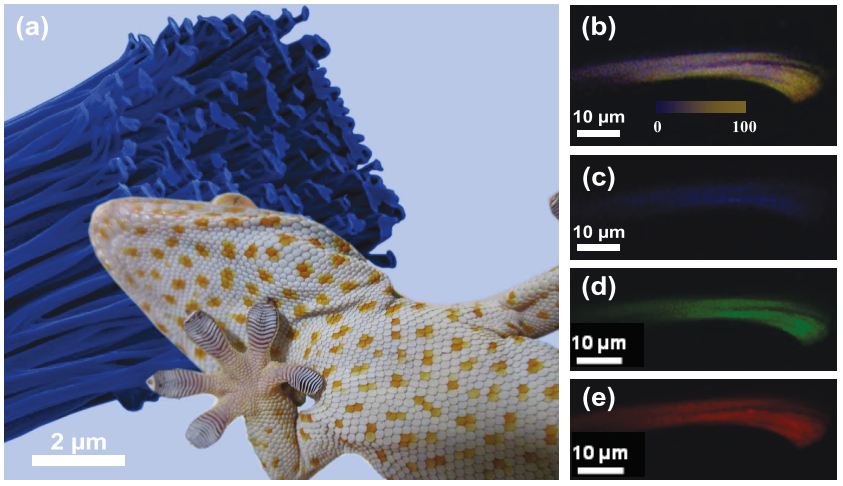

Figure 1. (a) Picture of a Tokay gecko sticking to an acrylic glass with the background showing the top part of a single seta; (b) confocal laser microscope (CLSM) image of single gecko seta, showing an overlay image of three different autofluorescence of (c)−(e). The overall colors become more intense from the base to the tip (i.e., from left to right in (b)), suggesting that there is an increasing amount of β-keratin from the base to the tips. Therefore, there is a gradient density distribution along the seta, consequently leading to gradient in mechanical properties. (c)−(e) CLSM images of seta with single excitation wavelengths of 458, 561, and 633 nm, respectively.

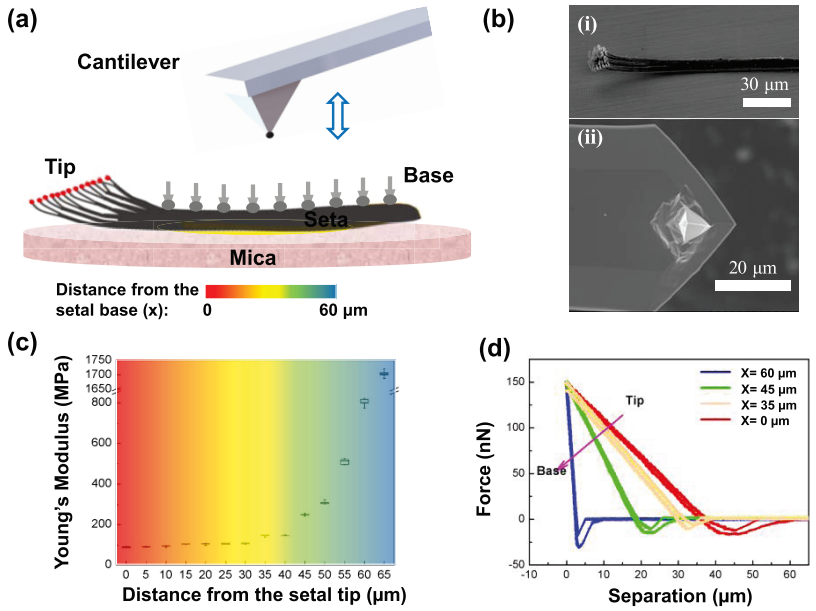

Figure 2. (a) Schematic of the AFM nanoindentation tests of single gecko seta at different setal stalk positions; (b) scanning electron microscopy (SEM) image of the seta morphology and the AFM carbon probe used in the test; (c) calculated gradient distribution of the Young's modulus of the single seta based on the AFM force curve obtained at varied longitudinal positions; and (d) the raw data (i.e., force−separation curves) used in (c).

roughness, to efficiently collect water from fog.[27] In addition to the structural gradient, chemical gradient coupled with laterally graded physical properties was revealed in ladybird beetle *Coccinella septempunctata*.[5] Its adhesive tarsal setae show a Young's modulus ranging from 1.2 MPa at the tip to 6.8 GPa at the base.

In the present work, we found that gecko setae are a functionally graded material, in which the Young's modulus gradually decreases from setal base to setal tip over 20 times in magnitude. We further showed through the finite element analysis (FEA) simulation that the gradient along the setal stalk significantly increases its contact compliance (critical for producing large frictional adhesion on rough surfaces) and reduces the stress concentration in the setal stalk (critical for achieving high fatigue resistance). The gradient modulus in combination with the hierarchical toe pad structure allows the gecko hairs to have both high adhesion and long fatigue life, leading to geckos' spectacular locomotion capabilities. Inspired by the gradient setae, we developed a facile benchmark method to fabricate functionally graded fibrillar adhesive arrays with improved adhesive performance and fatigue resistance.

2. RESULTS AND DISCUSSION

2.1. Functionally Graded Setae. A gecko toe pad has millions of small hairs named setae, and each seta further branches into hundreds of smaller hairs named spatulae. Figure 1a shows the toe pad structure of a live Tokay gecko sticking to an acrylic glass surface, with the spatulae as the background.

https://dx.doi.org/10.1021/acsapm.0c00282
ACS Appl. Polym. Mater. 2020, 2, 2658−2666

The confocal laser microscope (CLSM) image in Figure 1b, which is the combination of Figure 1c−e, provides clear evidence of the gradient distribution of elastic protein resilin (β-keratin) aligned in the longitudinal direction of a single seta.[5] In the middle of the seta, the material composition is strongly dominated by resilin, whereas in the distal portion of the seta (toward the right-hand side of each seta in Figure 1b−e), other proteins exist, assuming a smooth transition from one kind to the other. This effect is indicated by the dominant green and red autofluorescence in these structures (Figure 1c−e).[5] It is hypothesized that the gradient distribution of different proteins along the setae contributes to their robustness under cyclic loadings, as will be discussed in later sections.

To quantitatively analyze the gradient distribution, we harvested fresh setae from a live gecko, isolated single seta, and immediately glued it tightly onto a piece of freshly cleaved mica sheet. The Young's modulus of the setae was measured with an atomic force microscope (AFM), and the "nano-indentation" procedure is depicted in Figure 2a. Equations 1 and Equations 1 (in Section 4) are adopted to calculate the Young's modulus. We have calibrated the modulus on a standard material using the same tip. The moduli of dried and fresh seta are almost identical (Figure S1). We chose different positions along the longitudinal direction of the setal stalk to obtain the force curves and then the Young's modulus. The color bar under the schematic shows a direct correlation of the stiffness distribution along the sample. Force−separation curves on different positions of the setal stalk are shown in Figure 2c,d. As shown in Figure 2d, the setal stalk exhibits a distinct gradient distribution of Young's modulus in the longitudinal direction. This effect is reported for the first time in the gecko adhesive system, though it has been demonstrated previously that the gecko setae mainly consist of β-keratin.[28] A gecko seta is much stiffer and more rigid toward the proximal position at the base (x = 65 μm), whereas it is much softer toward the distal region at the tip (x = 0 μm, close to spatulae branches). The data points in Figure 2c highlight the smooth transition of the stiffness in gecko setae, similar to that of *C. septempunctata* but with different slope/curvature.[5] The Young's modulus of the setal base (1725 MPa) measured was nearly 20 times higher than that close to the tip (95 MPa). We have avoided the measurement from the small roots sticking out of the setal base, to exclude any complication from the structural hierarchy. The adhesion/cohesion energy of the single gecko setae on the surfaces was investigated using surface force apparatus (Figure S2).

2.2. Gecko-Inspired Functionally Graded Dry Adhesive Pillar Arrays. It is hypothesized that the excellent adhesive performance and longevity of natural gecko setae stem from their gradient modulus, which may be the missing piece in many synthetic dry adhesive arrays to date. To elucidate this effect and the underlying mechanism, we have fabricated functionally graded artificial dry adhesive micropillar arrays similar to gecko setae. The individual pillars are 10 μm in height and 10 μm in diameter. To obtain a gradient modulus distribution in the "artificial gecko setae," magnetic nanoparticles were incorporated into the poly(dimethylsiloxane) (PDMS) pillar matrices. Strong magnetic fields were applied to redistribute the evenly mixed nanoparticles in the matrices before the PDMS hardened, creating gradient moduli along the axial directions of each individual pillar.[29] Figure 3a−c shows the schematics of the fabrication process of the gradient micropillar arrays. The individual magnetic nanoparticles have

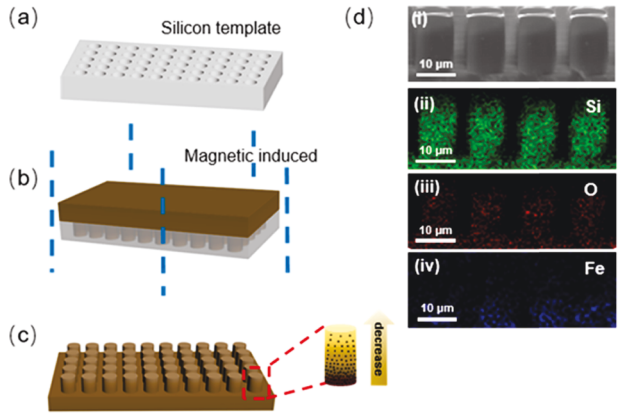

Figure 3. Schematics of the magnetically controlled molding processing: (a) the silicon template, (b) nanoparticle−PDMS mixture (colored brown) cast into the template (colored transparent gray), and (c) gradient PDMS-based pillar arrays obtained after demolding. (d) Images of cured pattern and elemental mapping: (i) SEM image of a single pillar; (ii) EDS images of the pillar, showing a gradient distribution of the magnetic particles; (iv) iron particles distribute gradient along the pillars, while the (ii) oxygen and (iii) silicon display the uniform distribution, which results in functionally graded pillars. The green, red, and blue dots represent silicon, oxygen, and iron elements, respectively.

a relatively uniform size distribution with a diameter of roughly 200 nm (Figure S3). The scanning electron microscopy (SEM) as well as energy-dispersive spectroscopy (EDS) images of one row of pillars are shown in Figures S4 and S5, respectively. Figure S6 shows the influence of magnetic field on the Young's modulus of the samples. The element mapping of the pillars shows a uniform distribution of the oxygen and silicon, but the iron element (corresponding to the Fe_3O_4 nanoparticles) displays a gradient distribution along the pillar longitudinal axis. Notably, the gradient distribution of these particles in the longitudinal direction leads to the gradient distribution of Young's modulus similar to the natural functionally graded setae, without introducing any structural hierarchy (e.g., from lamellae to setae, and to spatulae). We have measured the Young's modulus of a Fe_3O_4 particle uniformly distributed and gradient distributed in PDMS pillars (Figure 4). Since the Fe_3O_4 particles are much harder than the PDMS, the gradient pillars are softer at the tip but stiffer at the bottom like the natural setae. The EDS images of single pillar in Figure 3d confirm the gradient distribution of iron oxide

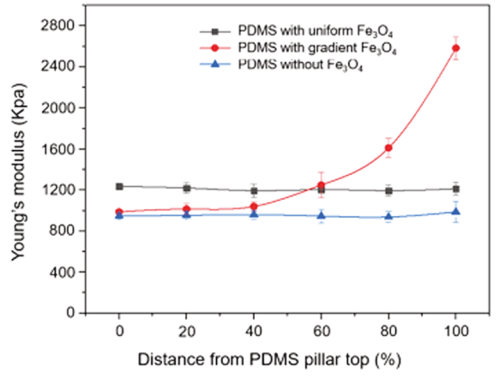

Figure 4. Young's modulus in the longitudinal direction of gradient and uniform PDMS with Fe_3O_4 and pure PDMS pillar without Fe_3O_4

https://dx.doi.org/10.1021/acsapm.0c00282
ACS Appl. Polym. Mater. 2020, 2, 2658−2666

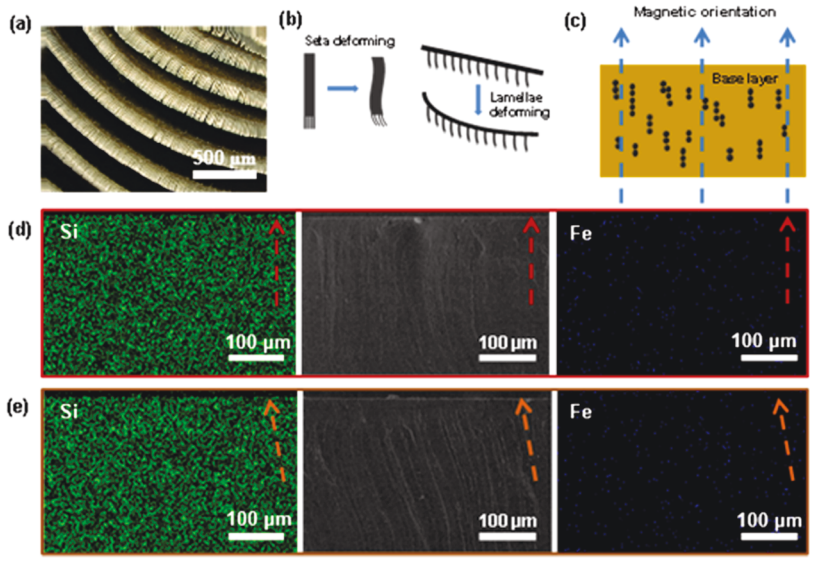

Figure 5. (a) SEM image of the gecko lamellar skin. (b) Schematic of the bending/conforming mechanism of gecko setae and lamellae during attachment. (c) Magnetically induced nanoparticle alignment. (d) SEM and EDS images of longitudinal cross-sectional area showing the particle alignment (0°; vertical). (e) SEM and EDS images of the longitudinal cross-sectional area showing the particle alignment (15°; tilted). The green and blue dots represent the silicon and iron elements, respectively. The inset arrows indicate the orientation of the applied external magnetic field.

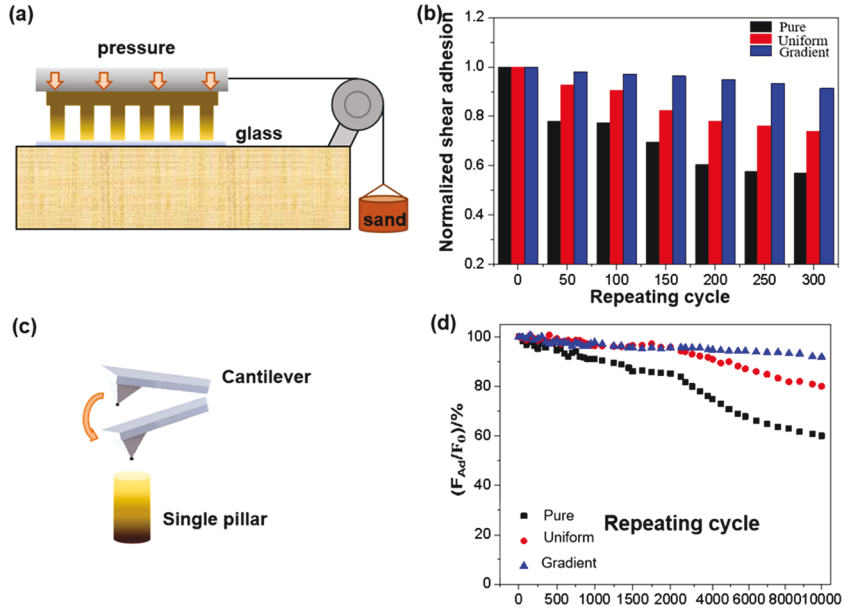

Figure 6. (a) Setup for measuring the macroscopic/device level (pillar arrays; 2 cm × 2 cm in size) shear adhesion of the biomimetic dry adhesives. (b) Shear adhesion force of the pillar arrays in 300 repeated tests for the pure, uniform, and gradient PDMS-based pillar arrays (corresponding to (a)). The uniform and gradient samples have the same doping ratio of Fe_3O_4 nanoparticles. (c) Setup for measuring microscopic level (individual pillar arrays; diameter of 10 μm and height of 10 μm) adhesion of the biomimetic dry adhesive pillars using AFM. (d) Adhesion durability tests on single pillar with up to 10 000 cycles of attachment−detachment (corresponding to (c)).

particles. The EDS line mapping along the longitudinal direction of single pillar has been performed with an accumulation time of 130 s. The results reveal that the relative intensity of the points on the top (0 μm), mid (5 μm), and bottom (10 μm) of a pillar has a ratio of 1:2:3. It is also worth noting from the water contact angle measurement (Figure S7) that the surface chemical composite was kept almost identical.

It is well known that gecko toe pads are multilevel structures, consisting of lamellar skin at the macroscale, setal arrays at the microscale, and spatulae brunching out from setal tips at the nanoscale (Figure 5a,b). Figure S8 shows the schematic of the deforming mechanism of the gecko setae. Besides the gecko setae and spatulae, lamellae offer additional levels of conformability at the highest level, to cope with the roughness of unpredictable daily surfaces. To imitate this hierarchical design, researchers have fabricated mushroom-shaped pillars on discretely supported thin films such that the deformation of the contact elements can be partially transferred to and absorbed by the noncontinuous base.[30]

Herein, we manipulated the magnetic particles by the external magnetic field to make additional levels of anisotropy and conformability in individual pillars. Specifically, as shown in Figure 5c, controlling the direction of the external magnetic field can feasibly change the particle aggregation orientation.

https://dx.doi.org/10.1021/acsapm.0c00282
ACS Appl. Polym. Mater. 2020, 2, 2658−2666

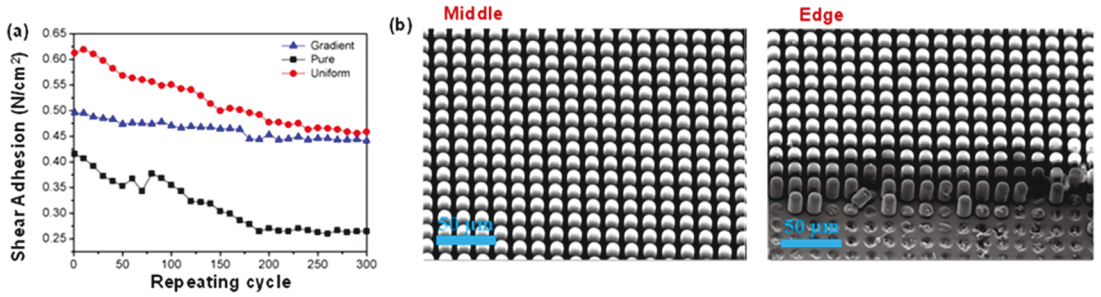

Figure 7. (a) Shear adhesion vs the repeating cycle of gradient, pure, and uniform pillars (b) SEM images of the middle and edge positions of uniformly distributed sample after 300 cycles of attachment−detachment.

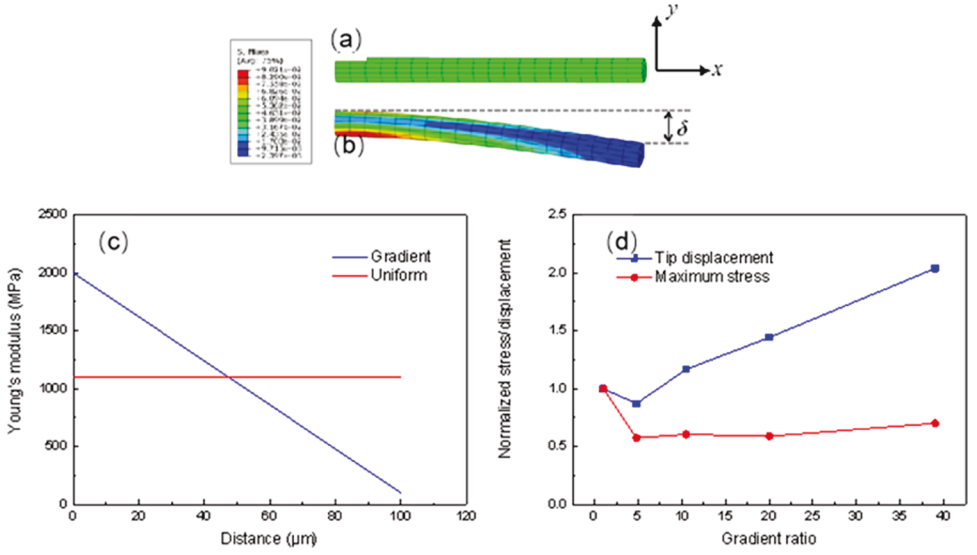

Figure 8. Snapshots of the finite element model of a gradient cylindrical pillar (cantilever) that is 100 μm long (along the x direction) and 8 μm in diameter (along the y direction): (a) initial unloaded state and (b) under shear loading F in the transverse direction the pillar's free end/tip deflect downward in the negative y direction by δ. (c) An example of the Young's modulus distribution in gradient and uniform cantilevers from base to tip and (d) the normalized free-end/tip displacement (blue curve) and the normalized maximum von Mises stress in the cylindrical pillar as a function of the gradient ratio. The gradient ratio is defined as the ratio between moduli of the fixed end vs the free end. The free-end displacement and maximum stress in the pillar are normalized with the corresponding values of the pillar with identical geometry (100 μm long and 8 μm in diameter) but constant/uniform modulus. The moduli of the uniform pillars (used to normalize the data) are set to be the average values of the gradient pillars for each specific gradient ratio, respectively.

The nanoparticles tend to aggregate along the magnetic induction line, evident by the SEM images and the iron element signal images in Figure 5d,e. We have fabricated the base layer of the dry adhesive surfaces with gecko lamella-like structures. The base layers were fabricated under: (1) vertical magnetic field and (2) a field with ~20° of tilt. SEM and EDS images in Figure 5d show a homogeneous distribution of Si, while the nanoparticles obviously orientated along the magnetic field induction direction, giving the base layers not only a rigid skeleton but also good conformability along the vertical direction compared to a uniformly distributed composite substrate. When the tilted distribution of nanoparticles or anisotropy is introduced, under normal engagement in the out-of-plane direction, the substrate can undergo larger deformation (less stress concentration) to absorb/alleviate more compressive loadings and energy than the one with 0° of tilt. It is expected that this effect will significantly improve the adhesion strength on rough surfaces and reduce adhesive damage.

As mentioned above, we have fabricated the gecko-inspired surface with gradient micropillars. The functionally graded pillars and lamella-like base have been confirmed by the EDS analysis. We tested our gradient patterns using a conventional method,[31] as illustrated in Figure 6a. In the test, a moderate preloading pressure of 0.25 N/cm^2 was applied to the gradient patterns on a glass surface, to avoid plastic deformation (Figure S9). The shear loading was then applied to the gradient patterns and gradually increased until sliding occurred. Figure 6b shows the shear adhesion against the loading cycles for the pillar arrays (Figure 6a). Interestingly, the uniformly distributed pattern showed the highest shear adhesion among all of the patterns at the initial stage but dropped significantly in only 50 cycles and then leveled off. The shear adhesion of pure PDMS sample also dropped by a large extent after 100 cycles. Among these samples, the gradient pattern exhibits the highest performance in terms of durability. We further implemented a durability test on a single pillar with a SiO_2 particle modified AFM tip. The contacts (attachment and detachment) between the pillar top surface and the SiO_2 particle were imposed repeatedly, as schematically shown in Figure 6c. We have tested 10 000 cycles of attachment−detachment for the single-pillar arrays (Figure 6d). It is evident that the single pillar with gradient distribution can maintain the highest original adhesion force after several experiments.

https://dx.doi.org/10.1021/acsapm.0c00282
ACS Appl. Polym. Mater. 2020, 2, 2658−2666

Figure 7 shows the adhesion test of the pillar arrays and SEM images of the uniform sample after 300 cycles. The results (Figure 7a) show that the pure PDMS patterns are less durable than the gradient and uniform ones. This is consistent with our previous works.[32,33] The Fe_3O_4-doped composite pillars (i.e., 2 wt %) with lower stiffness at pillar tip had a higher adhesion strength. The shear adhesive force of the gradient pillars was slightly lower than that of the uniform ones presumably due to the magnetic redistribution process of the magnetic particles. However, after 300 loading cycles, the gradient pillar arrays kept up to 90.7% of initial adhesion while the uniform and pure PDMS pillar arrays only maintained 74 and 57% of the initial adhesion forces, respectively (Figure 6a,b). In the single-pillar test, the gradient pillar maintained 91% of its initial adhesion after 10 000 cycles of attachment−detachment, while the uniform distributed pillars and pure PDMS pillars only maintained 80.1 and 60.2% of initial adhesion forces, respectively (Figure 6c,d). Besides, the gradient pillar shows intact SEM images, as shown in Figure 7b, while the uniform pillar shows break at the edges.

2.3. Finite Element Analysis of Gradient vs Uniform Micropillars. To gain an insight into the mechanism of the robustness and longevity of the adhesive fibrils featuring functional gradient, finite element analysis (FEA) simulations were conducted to calculate the stress and deformation of pillars under each loading cycle. As shown in Figure 8a, the gradient pillars (with identical dimensions and geometries) are modeled as a solid cylindrical cantilever beam with length 100 μm and diameter 8 μm. A cantilever beam with uniform Young's modulus and geometrically identical to the gradient one is also generated for comparison. The beams are mashed into 20 regions longitudinally and then assigned with gradient Young's modulus ranging from 100 to 5000 MPa and a Poisson's ratio of 0.5. Here, we define a parameter, gradient ratio, i.e., the ratio between the modulus of the fixed end and that of the free end of the cantilever beam, as a measure of the degree of gradient. For instance, when the gradient ratio is 20, the modulus of the gradient beam decreases linearly from 2000 to 100 MPa, from the fix end to the free end longitudinally (Figure 8c).

Figure 8b,d shows the von Mises stress concentration distribution and the maximum stress and tip displacement as a function of the gradient ratio, respectively. The maximum von Mises stress in the beam and the maximum displacement at the free end are normalized by the corresponding values of beams with identical dimension/geometry but with "uniform" modulus under the same shear loading. The modulus of the uniform beam used to normalize the data (i.e., maximum stress and free-end deflection) is set to be the average modulus of the gradient beam. For instance, when the gradient ratio is 20, the modulus of the gradient beam decreases linearly from 2000 to 100 MPa, from the fix to the free ends longitudinally, while the uniform beam used for normalizing this data point is set to be $(100 + 2000) \div 2 = 1050$ MPa. As shown in Figure 8d, as the gradient ratio increases, the normalized maximum stress decreases first and keeps at a constant value (slightly above 0.5), while the normalized free-end deflection is increased two times (from 1 to slightly above 2). Thus, functionally graded beams are more compliant (i.e., higher shear-induced deflection) and have much lower stress concentrations than the uniform ones under the same shear loadings. With these attributes, functionally graded beams will perform better on rough surfaces and are more durable under cyclic shear loadings than the uniform counterparts. Although there is no direct evidence showing that the gradient significantly improves the life cycles and makes the setae more durable (because there is no uniform natural seta), it has been shown experimentally that functionally graded cellular pillars have high fatigue strength and energy adsorption, which is superior to the uniform structures.[34]

Specifically, the higher the shear-induced deflection, the larger the real contact area will be generated between the tip free end and the opposing surface. This will result in higher levels of frictional adhesion,[35] especially for rough surfaces. Data shown in Figure 8d indicate that the gradient beam will perform better than their uniform counterparts in terms of both adhesion strength and longevity under cyclic shear loadings. When same levels of shear/frictional forces are applied by the "load and drag" procedure in each engagement loading cycle, the maximum stress (or stress concentration) developed in the gradient pillar is much lower than that of the uniform counterparts (~50%), while the deflection on the tip/free end of the gradient pillar is increased to more than two times. The lower stress of the gradient pillar would significantly contribute to its high fatigue life. Thus, variation in the mechanical properties of seta enhances contact compliance (on top of the geometric/structural hierarchy, e.g., from lamellae to setae and to spatulae), while retaining great robustness against bending-induced fracture. This phenomenon serves as an intriguing inspiration to increase the longevity of synthetic high-aspect-ratio fibrils that are constantly under cyclic and dynamic loadings. Hence, the gradient modulus is hypothesized to be the key factor for achieving robust adhesion and high fatigue resistance, seen in the gradient gecko setal stalks and the synthesized artificial nanocomposite mimics (i.e., Fe_3O_4/PDMS). Other factors, e.g., crack-resisting mechanism due to the mismatch at the reinforcements and matrix interfaces may also contribute to the longevity of heterogeneous micro-/nanopillars/fibrils, which will be investigated in future studies.

Notably, geckos use a load and drag procedure to engage the strong "frictional adhesion." The larger the setal stalk deflects at the tips/free end, the more real contact area it can generate between the spatula branches and the opposing surface. With the gradient modulus, if same levels of deflection are induced on the free end, stresses developed at the setal base are much lower than that of hypothetically uniform gradient stalks, making each seta extremely robust and sturdy.

Density functional theory (DFT) simulations have been implemented to further analyze the molecular mechanisms between the PDMS matrices and the gradient distributed Fe_3O_4 nanoreinforcements. The molecular structure of the PDMS matrix is modeled by the dimethyl siloxane polymerase chain, as shown in Figure 9a, while the structures of gradient PDMS pillars are modeled by the dimethyl siloxane polymerase chain jointed with Fe^{2+}, Fe^{3+} ions, and with both Fe^{2+} and Fe^{3+}, as shown in Figure 9b−d, respectively. Formation energies of these four structures shown in Figure 9a−d are −3.24, −7.37, −11.27, and −16.37 eV, which indicate the increasing stability from nonjointed structure to single- and to dual-jointed Fe_3O_4-containing PDMS. These results indicate that as the concentration of Fe_3O_4 in individual PDMS pillars is increased from the tip to the base, increasingly more PDMS molecules tend to bond with Fe^{2+} and Fe^{3+} via divalent iron cation, making the pillar stronger and stiffer from the tip to the base. As discussed above, this changing in mechanical/material

https://dx.doi.org/10.1021/acsapm.0c00282
ACS Appl. Polym. Mater. 2020, 2, 2658−2666

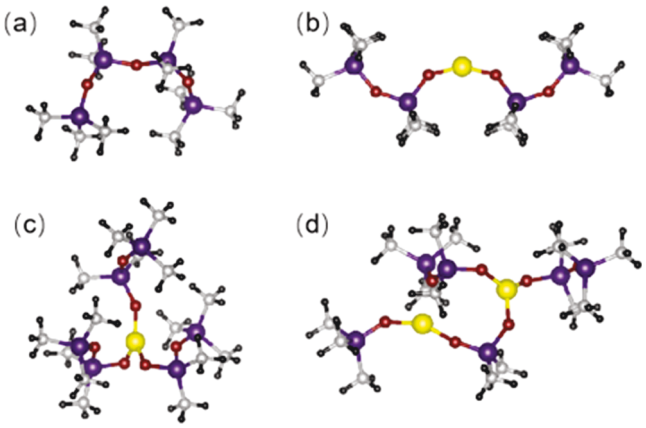

Figure 9. (a) Dimethyl siloxane polymerase chain, (b) two dimethyl siloxane polymerase chain jointed with one Fe^{2+}, (c) three dimethyl siloxane polymerase chains jointed with one Fe^{3+}, (d) dimethyl siloxane polymerase chain jointed with one Fe^{2+} and one Fe^{3+}. The purple, red, yellow, gray, and black balls represent Si, O, Fe, C, and H atoms, respectively.

properties greatly contributes to the robustness and fatigue resistance of the gradient synthetic adhesive pillars seen in the adhesion durability tests.

3. CONCLUSIONS

To the best of our knowledge, the present work reveals for the first time that individual gecko setal stalk has optimized modulus gradient for achieving robust adhesion with great durability and reusability. This natural design enables the elastic hairs to be both flexible toward the tips (critical to initiate strong frictional adhesion) and rigid at the base (key to achieve high fatigue resistance). The AFM tests show that the Young's modulus of a single setal stalk gradually reduces from the base to the tip by nearly 20 times in magnitude. We have fabricated biomimetic dry adhesives of gradient micropillar arrays through a facile method, by incorporating gradient distributed magnetic nanoparticles. The artificial gradient adhesives inspired by the natural setae were tested and characterized on both the macroscopic level (pillar arrays) and the microscopic level (single pillar). The results on the shear adhesion force (i.e., the pillar arrays) demonstrate that the gradient pillar adhesives are significantly more durable than the pure PDMS and the uniformly distributed pillar arrays. The adhesion forces of three different samples (i.e., individual pillars which are pure, uniform, and gradient) were measured with an AFM probe. At this microscopic level (i.e., single pillar), the gradient samples are demonstrated to be more durable than the pure PDMS pillars, but its cyclic adhesive performance is comparable to the uniformly distributed pillars. FEA simulation reveals that variation in the mechanical properties of natural setae and gradient micropillars is the key to enhance contact compliance (on top of the geometric/structural hierarchy, e.g., from lamellae to setae, and to spatulae), while retaining great robustness against bending-induced fracture and failure. This phenomenon serves as an intriguing inspiration to increase the longevity of synthetic high-aspect-ratio fibrils that are constantly under cyclic and dynamic loadings. This work paves the way for fabricating gecko-inspired dry adhesive arrays with extraordinary adhesive performance and longevity.

4. EXPERIMENTAL SECTION

4.1. Confocal Laser Scanning Microscopy (CLSM) Imaging. Freshly harvested gecko setae were transferred to glycerine (Z99.5%, free of water, two times distilled, Carl Roth GmbH & Co. KG) and mounted using high-precision coverslips. Then, the autofluorescence of gecko setae was analyzed using the confocal laser scanning microscope TCS SP8 (Leica, Germany) equipped with an inverted microscope and two solid-state lasers (wavelengths: 561 and 633 nm) and an argon laser (wavelengths: 458, 488, and 514 nm). For the visualization, a 40× objective lens (HCX PL APO CS 40× 1.30 OIL, 506358, Leica, Germany) was used.

4.2. Preparation of Single Gecko Setae. Setal arrays (dead skin of gecko) were collected from Tokay geckos and immediately stored in a sealed container to prevent contamination from dust and moisture. Fresh mica sheets were cleaved and glued on the top of a glass substrate under UV curing glue and ready for use. First, individual setae were isolated from setal arrays with micromanipulator installed inside the atomic force microscope (Scan-Icon AFM, Bruker Co., Inc.) with a tipless cantilever (ACTA-TL-50, AppNano) and glued onto the cylindrically curved surface of a silica disk with cyanoacrylate adhesive (Loctite 410, Henkel Loctite Corp., Rocky Hill, CT), with spatula facing up and mounted as the substrate surface in the surface forces apparatus (SFA) (SFA 2000, SurForce LLC, Santa Barbara, CA), 3.8 N/m. All of the process was operated in a clean room to prevent the contamination of the freshly cleaved mica surfaces. The glued setae were cured for 24 h in the SFA chamber before the tests.

4.3. Fabrication of PDMS Samples. First of all, silicon wafer with patterned holes was fabricated through a conventional photolithography process. Then, a mixture (10:1 base monomer-to-cross-linker ratio) of PDMS resin and magnetic nanoparticles was poured into the silicon mold for a specific amount to achieve certain desired thickness. Then, after degassing in a vacuum dryer for 10 min, the PDMS was cured in a lab-made large oven at 60 °C for 24 h and finally peeled off carefully. A magnetic field (VSM Model 8600, Lakeshore, OH) was applied (between −10 and 20 kOe at 20 °C) to redistribute the magnetic particles while curing to concentrate more toward the base of the pillars so that setae-like gradient pillars could be formed before curing and peeling off. The ultimate tensile strengths of pure and uniform PDMS is 846.849 and 1669.978 kPa, respectively, and the moduli of pure PDMS, uniform PDMS with Fe_3O_4, and gradient PDMS with Fe_3O_4 are 949, 1248, and 980−2583 kPa, respectively (Figure 4). The diameter of the Fe_3O_4 particle is around 20 nm average

4.4. Measuring Adhesion and Cohesion Energies. The adhesion/cohesion energy of the single gecko setae on the surfaces was investigated in surface force apparatus (SFA). One molecular-smooth freshly cleaved back-silvered mica sheet was glued on cylindrical glass disks with a radius of curvature of around 2 cm, which was used as a hydrophilic substrate. Another freshly cleaved mica surface was then treated with molecular vapor deposition (MVD) of heptadecafluro-1*H*, 1*H*, 2*H*, 2*H*-hydradecyltrichlorosilane (FDTS) using the MVD system (Applied MST, San Jose, CA) and used as hydrophobic surfaces. The contact angles of pristine mica and the FDTS-treaded one were measured as <10 and 140°, respectively. Detailed operation principles of the SFA were discussed elsewhere.[36] Briefly, surface separation can be measured down to 0.1 nm by employing an optical multiple beam interference technique. During the loading process, the setae at the terminal part of the seta was controlled to approach, make contact, and retreat at a controlled pulloff speed in the range of 1−100 nm/s. The temperature was controlled at 23 ± 1 °C, and the environment humidity was kept at 33% in all of the tests.

The Young's modulus was calculated based on our experiment results through a traditional hertz model between a spherical indenter and an elastic half-space by

$$E = \frac{3}{4}\frac{F(1-nu^2)}{\sqrt{R}d^{3/2}} \quad (1)$$

https://dx.doi.org/10.1021/acsapm.0c00282
ACS Appl. Polym. Mater. 2020, 2, 2658−2666

where E is the Young's modulus, F is the force, nu denotes Poisson's ratio, R represents the radius of the indenter, and d is the indentation depth. The Young's modulus is also calculated by

$$E\ (\mathrm{N/mm^2}) = \frac{1-\mu^2}{2RC_3}\left(\frac{C_1 + C_2 Sh_A}{100 - Sh_A}\right) \quad (2)$$

where constants C_1, C_2, and C_3 have values of 0.549 N, 0.07516 N, and 0.025 mm, respectively; R is the radius of the durometer's indenter (R = 0.395 mm); μ is Poisson's ratio (known as 0.50); and Sh_A is the material inner value.

4.5. Finite Element Analysis of Uniform/Gradient Pillars. Abaqus (version 6.11) was used to make finite element analysis of the mechanical behavior of setae and uniform/gradient pillars under shear loadings. The uniform setal stalk has the size of 8 μm in diameter and 100 μm in length (Figure S5a) and the Young's modulus and Poisson's ratio are 100−5000 MPa and 0.5, respectively. The "gradient" setal stalk has the same size as the uniform one, and its modulus linearly increases from 100 MPa at the tip to a certain value (100−5000 MPa) at the root such that its average modulus is the same as the uniform one. The root of seta is fixed while the tip is imposed to a force in the direction perpendicular to its axis.

■ ASSOCIATED CONTENT

Supporting Information

The Supporting Information is available free of charge at https://pubs.acs.org/doi/10.1021/acsapm.0c00282.

Young's modulus of the dried and fresh seta as a function of storage time; SFA force test; XRD, TEM, SAED, EDS mapping, and contact angle measurement of the surface; schematic of the hierarchical conforming deformation and behavior of the gecko adhesive system when contacting with rough surfaces; and adhesion force as a function of preloading pressure (PDF)

■ AUTHOR INFORMATION

Corresponding Authors

Yu Tian − *State Key Laboratory of Tribology, Tsinghua University, Beijing 100084, China;* orcid.org/0000-0001-7742-5611; Email: tianyu@mail.tsinghua.edu.cn

Zhenhai Xia − *Department of Materials Science and Engineering, University of North Texas, Denton, Texas 76203, United States;* orcid.org/0000-0002-0881-2906; Email: Zhenhai.Xia@unt.edu

Quan Xu − *State Key Laboratory of Heavy Oil Processing, China University of Petroleum-Beijing, Beijing 201139, China;* orcid.org/0000-0003-2195-2513; Email: xuquan@cup.edu.cn

Authors

Xiaoxiao Dong − *State Key Laboratory of Heavy Oil Processing, China University of Petroleum-Beijing, Beijing 201139, China*

Rui Zhang − *State Key Laboratory of Heavy Oil Processing, China University of Petroleum-Beijing, Beijing 201139, China*

Melvin A. Ramos − *Department of Mechanical Engineering, California State University, Los Angeles, California 90032, United States*

Travis Shihao Hu − *Department of Mechanical Engineering, California State University, Los Angeles, California 90032, United States*

Zhihang Wang − *State Key Laboratory of Heavy Oil Processing, China University of Petroleum-Beijing, Beijing 201139, China*

Hong Zhao − *State Key Laboratory of Heavy Oil Processing, China University of Petroleum-Beijing, Beijing 201139, China*

Lipeng Zhang − *College of Energy, Beijing University of Chemical Technology, Beijing 100029, China*

Yiyang Wan − *Department of Materials Science and Engineering, University of North Texas, Denton, Texas 76203, United States*

Complete contact information is available at: https://pubs.acs.org/10.1021/acsapm.0c00282

Author Contributions

#X.D. and R.Z. contributed equally to this work.

Notes

The authors declare no competing financial interest.

■ ACKNOWLEDGMENTS

The authors thank National Nature Science Foundation of China (No. 51875577), Tribology Science Fund of State Key Laboratory of Tribology (No. SKLTKF16A06), US National Science Foundation (NSF) (Award No. 1662288), and US NSF PREM program (Award No. 1523588) for the supports.

■ REFERENCES

(1) Barthlott, W.; C, N. Purity of the sacred lotus, or escape from contamination in biological surfaces. *Planta* **1997**, *202*, 1.

(2) Chen, H.; Zhang, P.; Zhang, L.; Liu, H.; Jiang, Y.; Zhang, D.; Han, Z.; Jiang, L. Continuous directional water transport on the peristome surface of Nepenthes alata. *Nature* **2016**, *532*, 85−89.

(3) Maier, G. P.; Rapp, M. V.; Waite, J. H.; Israelachvili, J. N.; Butler, A. Adaptive synergy between catechol and lysine promotes wet adhesion by surface salt displacement. *Science* **2015**, *349*, 628−632.

(4) Zheng, Y.; Bai, H.; Huang, Z.; Tian, X.; Nie, F. Q.; Zhao, Y.; Zhai, J.; Jiang, L. Directional water collection on wetted spider silk. *Nature* **2010**, *463*, 640−643.

(5) Peisker, H.; Michels, J.; Gorb, S. N. Evidence for a material gradient in the adhesive tarsal setae of the ladybird beetle *Coccinella septempunctata*. *Nat. Commun.* **2013**, *4*, No. 1661.

(6) Scholz, I.; Barnes, W. J. P.; Smith, J. M.; Baumgartner, W. Ultrastructure and physical properties of an adhesive surface, the toe pad epithelium of the tree frog, Litoria caerulea White. *J. Exp. Biol.* **2009**, *212*, 155−162.

(7) Barnes, W. J. P.; Baum, M.; Peisker, H.; Gorb, S. N. Comparative Cryo-SEM and AFM Studies of Hylid and Rhacophorid Tree Frog Toe Pads. *J. Morphol.* **2013**, *274*, 1384−1396.

(8) Autumn, K.; Liang, Y. A.; Hsieh, S. T.; Zesch, W.; Chan, W. P.; Kenny, T. W.; Fearing, R.; Full, R. J. Adhesive force of a single gecko foot-hair. *Nature* **2000**, *405*, 681−685.

(9) Neubauer, J. W.; Xue, L.; Erath, J.; Drotlef, D.-M.; Campo, Ad.; Fery, A. Monitoring the Contact Stress Distribution of Gecko-Inspired Adhesives Using Mechano-Sensitive Surface Coatings. *ACS Appl. Mater. Interfaces* **2016**, *8*, 17870−17877.

(10) Autumn, K.; Gravish, N. Gecko adhesion: evolutionary nanotechnology. *Philos. Trans. R. Soc., A* **2008**, *366*, 1575−1590.

(11) Hansen, W. R.; Autumn, K. Evidence for self-cleaning in gecko setae. *Proc. Natl. Acad. Sci. U.S.A.* **2005**, *102*, 385−389.

(12) Zhang, C.; McAdams, D. A.; Grunlan, J. C. Nano/Micro-Manufacturing of Bioinspired Materials: a Review of Methods to Mimic Natural Structures. *Adv. Mater.* **2016**, *28*, 6292−6321.

(13) Autumn, K.; Sitti, M.; Liang, Y. A.; Peattie, A. M.; Hansen, W. R.; Sponberg, S.; Kenny, T. W.; Fearing, R.; Israelachvili, J. N.; Full, R. J. Evidence for van der Waals adhesion in gecko setae. *Proc. Natl. Acad. Sci. U.S.A.* **2002**, *99*, 12252−12256.

(14) Prowse, M. S.; Wilkinson, M.; Puthoff, J. B.; Mayer, G.; Autumn, K. Effects of humidity on the mechanical properties of gecko setae. *Acta Biomater.* **2011**, *7*, 733−738.

(15) Stark, A. Y.; Badge, I.; Wucinich, N. A.; Sullivan, T. W.; Niewiarowski, P. H.; Dhinojwala, A. Surface wettability plays a significant role in gecko adhesion underwater. *Proc. Natl. Acad. Sci. U.S.A.* **2012**, *110*, 6340−6345.

(16) Huber, G.; Mantz, H.; Spolenak, R.; Mecke, K.; Jacobs, K.; Gorb, S. N.; Arzt, E. Evidence for capillarity contributions to gecko adhesion from single spatula nanomechanical measurements. *Proc. Natl. Acad. Sci. U.S.A.* **2005**, *102*, 16293−16296.
(17) Chen, B.; Gao, H. An Alternative Explanation Of The Effect Of Humidity In Gecko Adhesion: Stiffness Reduction Enhances Adhesion On A Rough Surface. *Int. J. Appl. Mech.* **2010**, *02*, 1−9.
(18) Li, L.; Song, W.; Xu, M.; Ovcharenko, A.; Zhang, G. Atomistic insights into the loading − Unloading of an adhesive contact: A rigid sphere indenting a copper substrate. *Comput. Mater. Sci.* **2015**, *98*, 105−111.
(19) Jeong, H. E.; Lee, J.-K.; Kim, H. N.; Moon, S. H.; Suh, K. Y. A nontransferring dry adhesive with hierarchical polymer nanohairs. *Proc. Natl. Acad. Sci. U.S.A.* **2009**, *106*, 5639−5644.
(20) Yoon, H.; Jeong, H. E.; Kim, T.-i.; Kang, T. J.; Tahk, D.; Char, K.; Suh, K. Y. Adhesion hysteresis of Janus nanopillars fabricated by nanomolding and oblique metal deposition. *Nano Today* **2009**, *4*, 385−392.
(21) Tao, D.; Gao, X.; Lu, H.; Liu, Z.; Li, Y.; Tong, H.; Pesika, N.; Meng, Y.; Tian, Y. Controllable Anisotropic Dry Adhesion in Vacuum: Gecko Inspired Wedged Surface Fabricated with Ultra-precision Diamond Cutting. *Adv. Funct. Mater.* **2017**, *27*, No. 1606576.
(22) Song, S.; Drotlef, D.-M.; Majidi, C.; Sitti, M. Controllable load sharing for soft adhesive interfaces on three-dimensional surfaces. *Proc. Natl. Acad. Sci. U.S.A.* **2017**, *114*, E4344−E4353.
(23) Jiang, W.; Lei, B.; Liu, H.; Niu, D.; Zhao, T.; Chen, B.; Yin, L.; Shi, Y.; Liu, X. Fabrication of directional nanopillars with high-aspect-ratio using a stretching imprint process with a microcavity mold. *Nanoscale* **2017**, *9*, 2172−2177.
(24) Ye, Z.; Lum, G. Z.; Song, S.; Rich, S.; Sitti, M. Phase Change of Gallium Enables Highly Reversible and Switchable Adhesion. *Adv. Mater.* **2016**, *28*, 5088−5092.
(25) Qu, L.; Dai, L.; Stone, M.; Xia, Z.; Wang, Z. L. Carbon Nanotube Arrays with Strong Shear Binding-On and Easy Normal Lifting-Off. *Science* **2008**, *322*, 238−242.
(26) Liu, Z.; Meyers, M. A.; Zhang, Z.; Ritchie, R. O. Functional gradients and heterogeneities in biological materials: Design principles, functions, and bioinspired applications. *Prog. Mater. Sci.* **2017**, *88*, 467−498.
(27) Ju, J.; Bai, H.; Zheng, Y.; Zhao, T.; Fang, R.; Jiang, L. A multi-structural and multi-functional integrated fog collection system in cactus. *Nat. Commun.* **2012**, *3*, No. 1247.
(28) Jain, D.; Stark, A. Y.; Niewiarowski, P. H.; Miyoshi, T.; Dhinojwala, A. NMR spectroscopy reveals the presence and association of lipids and keratin in adhesive gecko setae. *Sci. Rep.* **2015**, *5*, No. 9594.
(29) Wang, Z.; Shi, X.; Huang, H.; Yao, C.; Xie, W.; Huang, C.; Gu, P.; Ma, X.; Zhang, Z.; Chen, L.-Q. Magnetically actuated functional gradient nanocomposites for strong and ultra-durable biomimetic interfaces/surfaces. *Mater. Horiz.* **2017**, *4*, 869−877.
(30) Hu, H.; Tian, H.; Shao, J.; Li, X.; Wang, Y.; Wang, Y.; Tian, Y.; Lu, B. Discretely Supported Dry Adhesive Film Inspired by Biological Bending Behavior for Enhanced Performance on a Rough Surface. *ACS Appl. Mater. Interfaces* **2017**, *9*, 7752−7760.
(31) Wang, Z. Slanted Functional Gradient Micropillars for Optimal Bioinspired Dry Adhesion. *ACS Nano* **2018**, *12*, 1273−1284.
(32) Li, M.; Xu, Q.; Wu, X.; Li, W.; Lan, W.; Heng, L.; Street, J.; Xia, Z. Tough Reversible Adhesion Properties of a Dry Self-Cleaning Biomimetic Surface. *ACS Appl. Mater. Interfaces* **2018**, *10*, 26787−26794.
(33) Li, M.; Li, W.; Cai, W.; Zhang, X.; Wang, Z.; Street, J.; Ong, W.-J.; Xia, Z.; Xu, Q. A self-healing hydrogel with pressure sensitive photoluminescence for remote force measurement and healing assessment. *Mater. Horiz.* **2019**, *6*, 703−710.
(34) Zhao, S.; Li, S. J.; Wang, S. G.; Hou, W. T.; Li, Y.; Zhang, L. C.; Hao, Y. L.; Yang, R.; Misra, R. D. K.; Murr, L. E. Compressive and fatigue behavior of functionally graded Ti-6Al-4V meshes fabricated by electron beam melting. *Acta Mater.* **2018**, *150*, 1−15.
(35) Autumn, K.; Dittmore, A.; Santos, D.; Spenko, M.; Cutkosky, M. Frictional adhesion: A new angle on gecko attachment. *J. Exp. Biol.* **2006**, *209*, 3569−3579.
(36) Israelachvili, J.; Min, Y.; Akbulut, M.; Alig, A.; Carver, G.; Greene, W.; Kristiansen, K.; Meyer, E.; Pesika, N.; Rosenberg, K.; Zeng, H. Recent advances in the surface forces apparatus (SFA) technique. *Rep. Prog. Phys.* **2010**, *73*, No. 036601.

https://dx.doi.org/10.1021/acsapm.0c00282
ACS Appl. Polym. Mater. 2020, 2, 2658−2666